npj Climate and Atmospheric Science https://doi.org/10.1038/s41612-026-01364-1

Article in Press

Satellite latent heating retrievals uncover a seasonal terrain-monsoon seesaw in southern Tibetan Plateau rainfall

Received: 20 September 2025

Accepted: 20 February 2026

Cite this article as: Zhou, Y., Li, R., Zhao, H. *et al.* Satellite latent heating retrievals uncover a seasonal terrain-monsoon seesaw in southern Tibetan Plateau rainfall. *npj Clim Atmos Sci* (2026). https://doi.org/10.1038/s41612-026-01364-1

Yan Zhou, Rui Li, Hongwei Zhao, Chun Zhao, Peng Zhang, Lin Chen, Qiong Wu, Yanluan Lin, Yunfei Fu, Yu Wang, Renjun Zhou, Lei Zhong & Xuanye Xu

Satellite Latent Heating Retrievals Uncover a Seasonal Terrain-Monsoon Seesaw in Southern Tibetan Plateau Rainfall

Yan Zhou[1#], Rui Li[1#,*], Hongwei Zhao[1], Chun Zhao[1], Peng Zhang[2,3], Lin Chen[3], Qiong Wu [3], Yanluan Lin[4], Yunfei Fu[1], Yu Wang [1], Renjun Zhou[1], Lei Zhong [1], Xuanye Xu[1]

[1] School of Earth and Space Sciences, Joint Laboratory of Fengyun Remote Sensing, University of Science and Technology of China, Hefei, China.

[2] Key Laboratory of Environment Characteristics and Effects for Near-space, Beijing, China.

[3] Meteorological Observation Center, China Meteorological Administration, Beijing, China.

[4] Ministry of Education Key Laboratory for Earth System Modeling, Center for Earth System Science, and Joint Center for Global Change Studies (JCGCS), Tsinghua University, Beijing, China.

# Equal contributions to this work

[*] Correspondence to rli7@ustc.edu.cn

Abstract

The relative roles of the Himalayan orography and South Asian summer monsoon (SASM) circulation in Tibetan Plateau (TP) precipitation remain contentious, yet numerical simulations exhibit substantial uncertainties due to extreme topographic gradients. Conventional satellites capture only exterior cloud properties or precipitation particle quantification, missing cloud-internal heating and updrafts. Using a novel satellite retrieval, we resolve the vertical structure of latent heating (LH) within precipitating clouds along the Himalayan slopes, offering new insight into precipitation drivers in this critical region. Satellite observations show that in spring, the altitude of peak latent heat (APLH) follows the southern slope topography, reflecting strong orographic control. Model results reveal that surface sensible heating below 2 km and orographic uplift above 2 km together enhance vertical motion and precipitation. In summer, however, the APLH stabilizes near 6 km across the southern Plateau, pointing to diminished local forcing and dominant large-scale monsoon control. The SASM supplies warm, moist air via mid-tropospheric moisture transport, bypassing terrain lifting and surface heating. These findings reveal a terrain-monsoon "seesaw" in Himalayan cloud-precipitation processes, characterized by a seasonal shift in dominance from local orographic forcing before the onset of the SASM to large-scale monsoonal circulation after the onset. This perspective provides broader insights into mountain-monsoon water cycle interactions worldwide.

Introduction

As Earth's largest and highest plateau, the Tibetan Plateau (TP) covers over 2.5 million km² with an average elevation above 4,000 m [1, 2]. This climate-sensitive region has experienced accelerated hydroclimatic shifts due to recent warming-wetting trends [3-8], with cascading effects on atmospheric circulation, ecosystems, and regional socioeconomic stability [9, 10].

The southern TP slope—a critical transition zone between the Indian Plains and the plateau—features an east–west–aligned megatopography. This region serves as a natural laboratory for probing interactions among mechanical forcing, thermal forcing, large-scale circulation, and precipitation. Orographic uplift drives low-level moist air ascent, enhancing condensation, latent heating (LH), and precipitation [11, 12], while slope-absorbed solar radiation fuels convective updrafts [13].

Beyond local-scale effects, debate persists regarding TP's role in the South Asian monsoon (SASM). The "TP thermal pump" theory posits that surface heating over the plateau drives large-scale air ascent from the Indian Ocean [13-15], whereas the "Himalayan barrier" hypothesis attributes SASM primarily to mechanical blocking of dry northerly flows and orographic uplift [16]. This unresolved 'Monsoon Melee' [17], concerning the relative importance of thermal pumping and mechanical blocking in sustaining SASM, partly stems from the inadequacy of coarse model resolutions to represent TP's complex terrain [18, 19]. Critically, whether TP's high-elevation thermal forcing can draw low-level moist air masses up steep slopes remains contested. Dong et al. [20] argued that moist air ascends remotely to ~6 km altitude before horizontal advection, bypassing slope ascent.

Clarifying the disputed thermodynamic–dynamic mechanisms under the Plateau's complex southern slope topography, as well as the interactions between local slope forcing and large-scale circulation, urgently requires new observational evidence. Most studies of TP precipitation have focused on large-scale or cloud-top features [21, 22], with little attention to the internal energy structure of precipitating clouds. Conventional satellite remote sensing captures precipitation particle states, but not dynamics-related vertical motions or thermodynamics-related LH. Here we leverage a breakthrough: Li et al. [23, 24] and Zhao et al. [25, 26] quantitatively derived LH profiles from precipitation-rate vertical profiles by spaceborne radar. This approach exploits the physical linkage that in saturated clouds, the LH is proportional to adiabatic cooling, which itself is proportional to the vertical velocity. Consequently, the LH profile provides an indirect measure of convection-scale updraft and downdraft velocities.

Using this method, we demonstrate that precipitation-associated LH is strongly coupled with southern TP slope topography in spring but decouples in summer. Crucially, the altitude of peak latent heat (APLH) tracks terrain elevation in spring (linear correlation: $r = 0.89$, $p < 0.01$), but stabilizes horizontally at 5–6 km in summer despite an elevation gain exceeding 4 km. This provides the first direct observational evidence of seasonal regime shift from local topographic thermodynamic and dynamic forcing to large-scale monsoonal dominance. Simulations further indicate that southern slope precipitation is sustained by altitude-dependent orographic and thermal forcing in spring precipitation process. This work reveals the concealed vertical structure of orographic precipitation, delivering observational constraints on surface-atmosphere-circulation

coupling over the southwestern Himalayas that are critical for refining atmospheric models and understanding regional hydroclimate responses.

Results

Vertical structure of satellite-derived latent heating in spring and summer

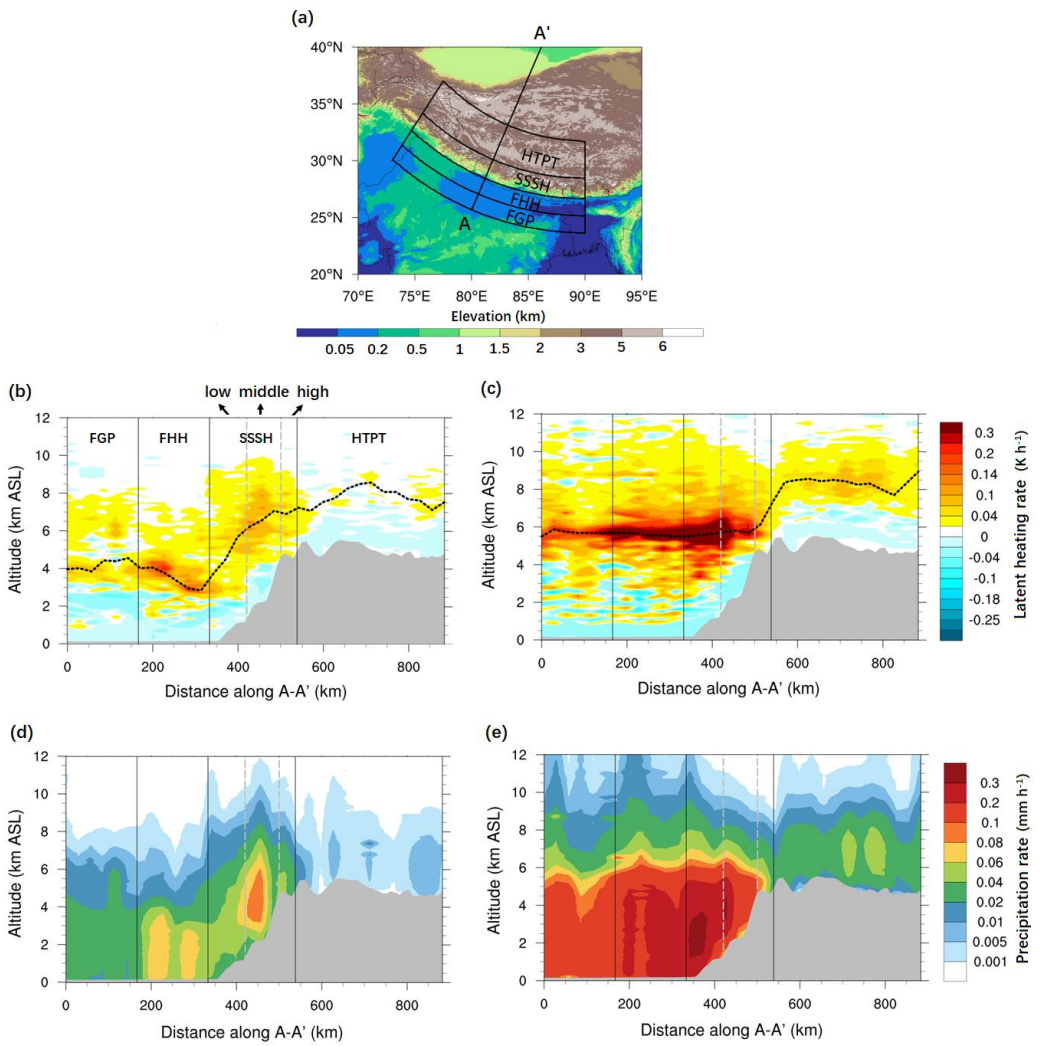

Figure 1 | Study domain and vertical structure of latent heating and precipitation over the southern Tibetan Plateau. (a) Topography showing four study regions: Flat Gangetic Plain (FGP), Foothills of the Himalayas (FHH), Steep Southern Slope of the Himalayas (SSSH), and Himalayan–Tibetan Plateau Tableland (HTPT). Transect A–A' marks the vertical cross-section location. (b, c) Multi-year (2014–2020) mean latent heating rate derived from GPM-DPR observations along A–A' for (b) spring (MAM) and (c) summer (JJA). Black dashed curves: altitude of peak latent heat. (d, e) Corresponding precipitation rate for (d) MAM and (e) JJA.

The southern Himalayan terrain exhibits extreme topographic gradients. Along our study transect (A–A' in Fig. 1a)—spanning the Flat Gangetic Plain (FGP), Foothills of the Himalayas (FHH), Steep Southern Slope of Himalayas (SSSH), and Himalayan–Tibetan Plateau Tableland (HTPT)—surface elevation rises from 0 km to ~5 km over a horizontal distance of ~300 km (mean gradient: 16.7 m/km). This steep slope serves as a primary barrier to northward moisture transport from the Arabian Sea and Bay of Bengal (Supplementary Fig. 1). Enhanced precipitation rates and LH over FHH and SSSH (Supplementary Figs. 2–3) indicate deep convective activity even during pre-monsoon spring.

Figure 1b reveals a terrain-dependent vertical structure of LH during spring (MAM). Along transect A–A', the altitude of peak latent heat (APLH) closely tracks surface elevation **(**linear correlation: $r = 0.89$, $p < 0.01$; based on grid points along transect A-A' **).** The two curves—APLH and surface elevation—show nearly parallel variations. This strong covariation indicates orographic dominance in precipitation processes. Sensitivity experiments (Fig. 4) further identify mechanical uplift as the primary driver (see *Mechanism Analysis*).

In contrast, during the summer, the vertical distribution of LH decouples from terrain (Fig. 1c). From the southern Indian plains all the way to the high parts of SSSH, the terrain rises by approximately 5 km, while the APLH shows a horizontally flat distribution, generally stable at altitudes of ~6 km. Horizontally, summer LH distributions show a monsoon-driven uniform heating belt extending from SSSH into India (Supplementary Fig. 3d). HTPT exhibits upper-level heating at 8 km and cooling below 7 km (Supplementary Figs. 3e, 3f), indicating net ascending motion in the upper atmosphere and subsidence below. These horizontal patterns suggest that HTPT precipitation is primarily driven by large-scale mid-upper moisture transport and atmospheric wave activity, rather than orographic lifting on the southern slope.

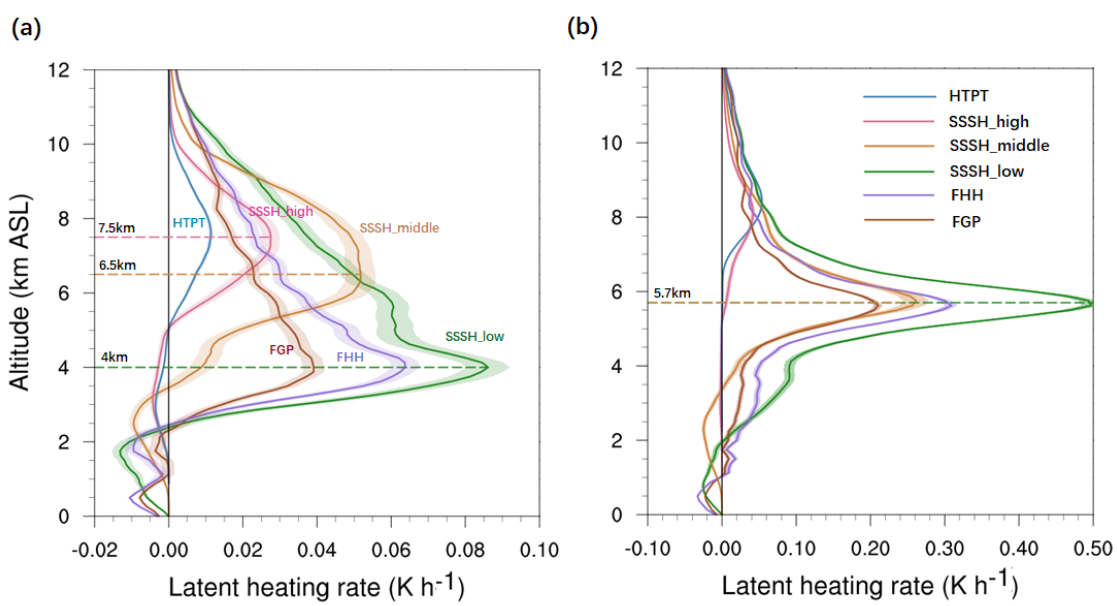

Figure 2 | Seasonal contrast in altitude of peak latent heat along the elevation gradient. (a) Spring (MAM) and (b) summer (JJA) mean latent heating rate profiles (2014–2020) for: **FGP (brown)**, Flat Gangetic Plain; **FHH (purple)**, Foothills of Himalayas; **SSSH_low (green)**, Lower Steep Southern Slope of Himalayas; **SSSH_middle (orange)**, Mid Steep Southern Slope of Himalayas; **SSSH_high (pink)**, Upper Steep Southern Slope of Himalayas; **HTPT (blue)**, Himalayan–Tibetan Plateau Tableland. Dashed lines: the altitude of peak latent heat. Shading denotes the 95% confidence interval of the mean (±1.96 standard error (SE)).

Regionally averaged LH profiles demonstrate distinct seasonal controls on APLH (Fig. 2). In spring, APLH increases progressively from 4.0 km over FGP, FHH, and SSSH-low to 6.8 km over SSSH-middle, reaching 7.5 km over SSSH-high and HTPT, which shows a near-linear elevation dependency. In summer, APLH remains statistically invariant at 5.7 km across FGP, FHH, SSSH-low, and SSSH-middle, while rising to ~8 km over HTPT—signifying distinct dynamical regimes: slope regions are decoupled from terrain due to monsoonal influence, whereas the plateau shows obviously increased APLH (~2km) due to large-scale topography.

Relationship between latent heating and reanalysis-based vertical motion

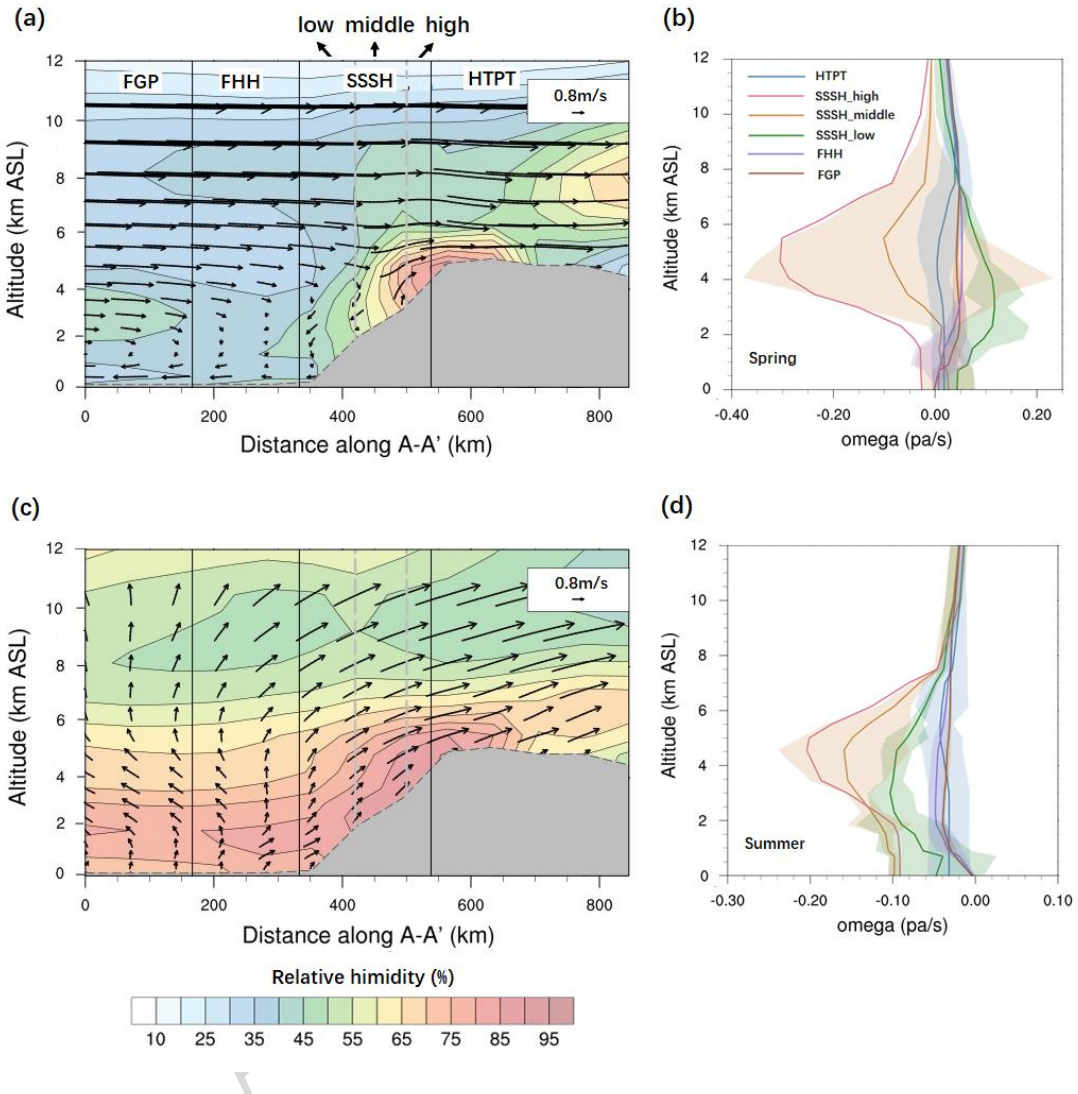

Figure 3 | Vertical structure of humidity and vertical motion over the southern Tibetan Plateau based on ERA5 data. (a, c) Relative humidity (shading) and horizontal wind vectors with vertical velocity scaled ×10 (arrows) along transect A-A' (Fig. 1a) for (a) spring (MAM) and (c) summer (JJA) during 2014–2020. (b, d) Regional mean vertical velocity (ω; Pa s^{-1}) profiles for: SSSH-low (green), SSSH-middle (orange), SSSH-high (pink), HTPT (blue) in (b) spring and (d) summer. Negative ω indicates upward motion. Shading denotes mean ± SE. The contrast demonstrates strong orographic forcing in spring versus monsoonal control in summer.

LH is linked to vertical gradients of precipitation rate [24], which in turn reflects vertical motion within convective clouds [23, 27]. ERA5 reanalysis data reveal that the altitude of maximum condensation (as indicated by APLH) coincides with the level of maximum updraft velocity. In spring, ERA5 indicates westerly advection of cold, dry air over the southern slope (Supplementary Fig. 1a,c,e), consistent with previous findings [28]. Over SSSH-low, low relative humidity (Fig. 3a) and downdrafts (Fig. 3b, green curve) indicate weak, shallow convection and light precipitation. Here, the downdraft signal over the lower slopes may partly arise from

resolution limitations [29, 30], where shallow updrafts are smoothed and potentially obscured by background subsidence linked to the large-scale Hadley circulation and the effects of topographic blocking. In contrast, over SSSH-middle and SSSH-high, updrafts dominate (Fig. 3b, orange and pink curves), likely due to orographic lifting, which drives significant precipitation (Fig. 1d). Vertical ascent velocity peaks at 5–6 km ASL over SSSH-high (Fig. 3b, pink curve), coinciding with the APLH (Fig. 1b).

In summer, deep convection is triggered by monsoonal depressions over central India [31-33]. This feature is evident in Supplementary Fig. 1c,d,f and drives strong updrafts across the FGP, FHH, and SSSH regions (Fig. 3c). Both peak LH and maximum vertical velocity occur at similar altitudes (~5 km ASL; Figs. 3d and 1c), with little variation across the slope—indicating that orographic effects are largely overridden by monsoonal circulation. Over HTPT, weak ascent and low moisture (Fig. 3, c and d) suppress convection, resulting in lower LH and precipitation than on the slope (Supplementary Figs.2-3).

WRF simulations of topographic, surface heating, and monsoonal influences on latent heating

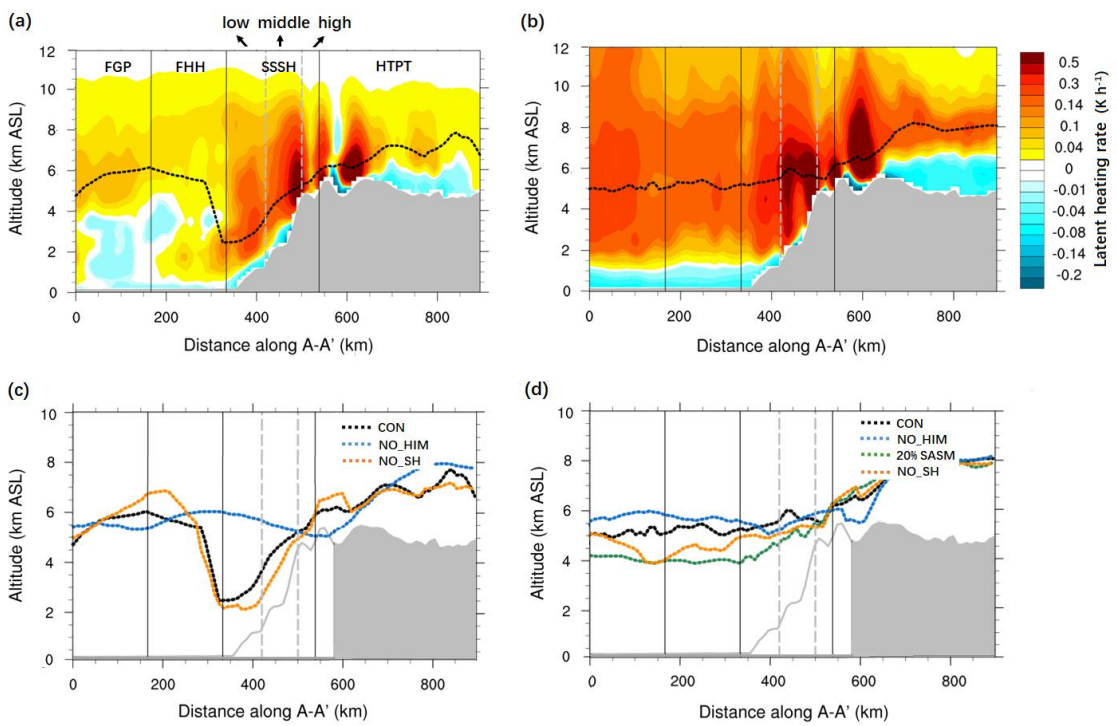

Figure 4 | WRF sensitivity experiments isolating controls on latent heating.

(a, b) Latent heating (LH) along transect A–A′ simulated in the control run (CON) for (a) s pring and (b) summer 2015. (c, d) Altitude of peak latent heat (APLH) under:
- **NO_HIM**: Remove Himalayan topography <5.5 km

- **NO_SH**: Disable surface sensible heating over slope
- **20% SASM**: Reduce South Asian Monsoon winds to 20% of control

(c) Spring APLH: CON (black dashed), NO_HIM (blue), NO_SH (yellow).
(d) Summer APLH: CON (black), 20% SASM (green), NO_SH (yellow).

Observational analyses alone cannot resolve the relative contributions of Himalayan orographic uplift, surface sensible heating (SH), and large-scale monsoon circulation to LH [17]. To address this mechanistic gap, we conducted targeted Weather Research and Forecasting (WRF) model simulations for 2015 (Methods; Supplementary Table 4). The control run (CON) accurately replicates observed precipitation patterns, as validated against GPM-DPR satellite data with root-mean-square error below 1 mm/day (Supplementary Fig. 5). Our experimental design employs three sensitivity configurations to isolate specific drivers: the NO_HIM experiment removes topography below 5.5 km to eliminate orographic mechanical forcing; the NO_SH experiment retains full topography but disables surface SH flux; and the 20% SASM experiment quantifies large-scale circulation impacts by reducing zonal (U) and meridional (V) wind components to 20% and moisture (QVAPOR) to 60% of control values throughout the atmospheric column. This monsoon wind reduction was implemented via boundary condition vector scaling in WRF, preserving spatiotemporal coherence while systematically reducing intensity to isolate monsoonal controls independent of local terrain and thermal effects.

The spring CON successfully reproduces the characteristic orographic modulation of APLH, demonstrating a progressive rise from 2 km over the lower slopes to 6 km at higher elevations along the southern Himalayan terrain (Fig. 4a). Analysis of three additional transects along the southwestern slope further substantiates that the APLH increases with terrain elevation across slopes of varying steepness (Supplementary Fig. 7). This elevation-dependent pattern arises directly from mechanically forced precipitation systems aligned with the steep topography, as evidenced by Supplementary Fig. 8a. When Himalayan topography is removed in the NO_HIM experiment, this orographic signature is fundamentally disrupted. The APLH stabilizes uniformly near 5 km with no observable elevation dependence (blue dashed curve, Fig. 4c), while orographic precipitation features are eliminated across the region (Supplementary Fig. 8c), and LH cores are completely absent (Supplementary Fig. 6c). These coordinated responses confirm that mechanical forcing constitutes the essential driver of springtime APLH elevation dependence.

Further mechanistic insights emerge from the NO_SH experiment, which retains full topography but disables surface SH. This configuration reveals a striking altitude dependence in controlling processes (yellow dashed curve, Fig. 4c). Below 2 km elevation, APLH completely decouples from terrain variations, maintaining a horizontal profile with decreased LH intensity—most prominently over the SSSH-low region (Supplementary Fig. 6e). This demonstrates the dominant role of surface SH in driving low-elevation convection. In contrast, above 2 km, APLH continues to track terrain elevation, with heating intensity reduced by less than 20%. This persistence confirms orographic lift as the primary control mechanism at higher altitudes. The large-scale LH patterns under NO_SH conditions further validate this altitude-stratified control framework (Supplementary Fig. 9e).

The physical mechanisms controlling springtime APLH variability were investigated using diagnostics of moisture and vertical motion. CON simulation shows lower moisture in spring than in summer across the study domain (Supplementary Fig. 10a), yet updrafts persist and intensify with Himalayan elevation (Supplementary Fig. 11a), confirming orographic dominance. Sensitivity experiments reveal divergent controls: topography removal (NO_HIM) nearly eliminates updrafts over the steep southern slope (Supplementary Fig. 11c), leading to suppressed convection despite available moisture (Supplementary Fig. 10c), while SH removal (NO_SH) weakens updrafts—especially below 2 km (Supplementary Fig. 11e)—reducing orographic precipitation over SSSH-low (Supplementary Fig. 8e). This demonstrates that moisture availability regulates precipitation potential, but mechanical forcing generates essential updrafts for orographic condensation, with SH modulating intensity at lower elevations.

The summer CON demonstrates a uniformly stable APLH near 6 km across the study region (Fig. 4b). To further justify whether the 10-km configuration adequately resolves monsoon precipitation over the Himalayas, we performed an additional 4-km control simulation for summer (Supplementary Fig. 12). The 4-km results show LH and APLH patterns broadly consistent with those in the 10-km simulation (Supplementary Fig. 12b, Supplementary Fig. 6b), supporting the adequacy of the 10-km resolution. When the SASM intensity is reduced by 80% (20% SASM experiment), substantial changes are observed: precipitation weakens over the SSSH, precipitation-top heights decrease, and precipitation distribution becomes increasingly terrain-dependent, resembling spring patterns (Supplementary Fig. 8d). This shift correlates with reduced moisture availability (Supplementary Fig. 10d), resulting in reduced LH intensity throughout northern India and the Himalayas, evident in horizontal and vertical distributions of LH (Supplementary Figs. 6d, 9d). The APLH profile (green dashed curve, Fig. 4d) descends by approximately 1 km over northern India due to suppressed updrafts (Supplementary Fig. 11d), then ascends following terrain elevation, demonstrating enhanced orographic control under weakened monsoon conditions.

In contrast, the removal of surface SH (NO_SH) or Himalayan topography (NO_HIM) minimally alters APLH terrain dependence in summer. The APLH profile of NO_SH (yellow dashed curve, Fig. 4d) remains closely aligned with the control run, and the horizontal distribution of LH remains largely unchanged (Supplementary Fig. 9f). However, this experiment reveals that SH contributes to convective intensity along the slopes, as its removal weakens slope convection (Supplementary Fig. 11f) and reduces LH magnitude (Supplementary Fig. 6f). Concurrently, enhanced moisture transport toward northern India elevates LH intensity in this region (Supplementary Fig. 10f). After removing the summer topography (NO_HIM), vertical velocity and LH intensity over the slope region decrease further relative to NO_SH (Supplementary Figs. 11g and 6g). However, the APLH still remains aligned with the LH center over the Indian subcontinent (blue dashed curve, Fig. 4d). These results indicate that the monsoon primarily determines the spatial pattern of LH over the slope region, whereas the heat-source effect of the elevated topography modulates LH intensity by influencing upward motion.

Discussion

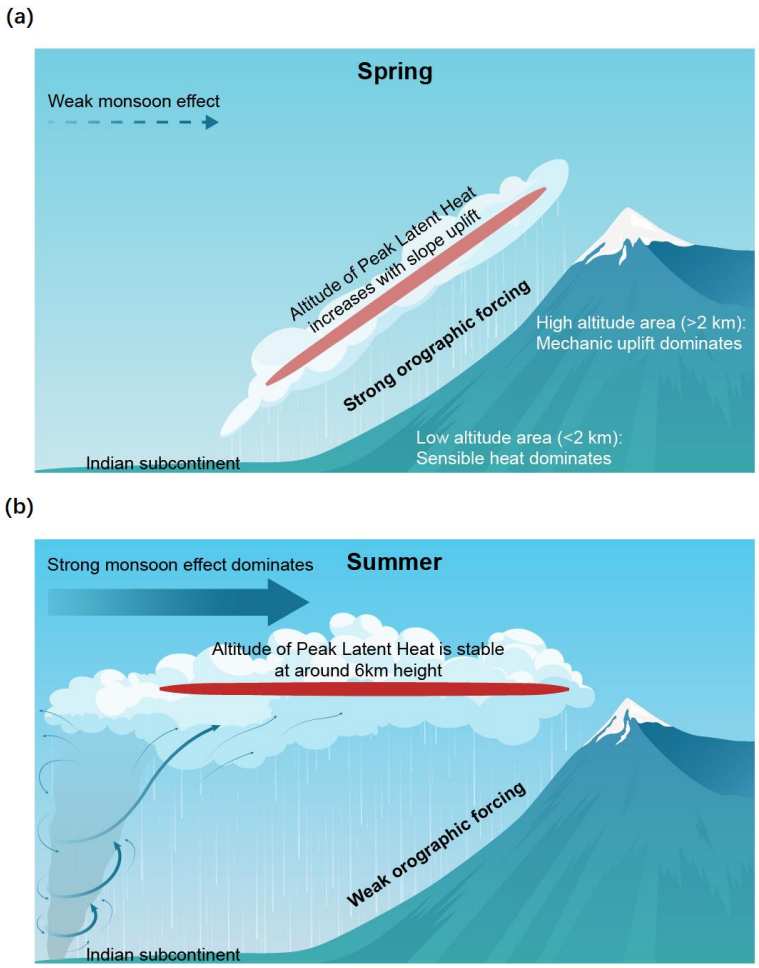

Figure 5 | A schematic of seasonal terrain-monsoon seesaw in dominant factors (local orographic forcing vs. large-scale monsoon forcing) for determining the distribution of precipitation and latent heating over the steep southern slope of Tibetan Plateau during (a) spring non-monsoon season and (b) summer monsoon season.

The dominant controls on precipitation over the southern TP slope have long been debated due to observational limitations: conventional optical remote sensing captures only cloud-top properties, while spaceborne precipitation radars quantify hydrometeor profiles but neither resolve vertical velocities nor capture cloud dynamics. This study overcomes these constraints through a novel application of satellite-derived LH rates—a quantity directly proportional to saturated-adiabatic vertical velocity—revealing distinct seasonal regimes in precipitation processes.

Our analysis provides the first direct observational evidence that springtime APLH tightly tracks terrain elevation, exhibiting near-parallel covariation along the slope. In summer, however, APLH stabilizes horizontally at 5–6 km across dramatically varying topography. Although summer daytime slope warming can strengthen thermally driven anabatic (upslope) winds [34, 35], such local effects are still suppressed at the scale of the seasonal mean by large-scale advection. The APLH remains largely terrain-independent in summer for both daytime and

nighttime conditions (Supplementary Fig. 13). Thus, the apparent decoupling of APLH from terrain also persists throughout the diurnal cycle.

To validate the observed results, the spectral latent heating (SLH) Version 07 product based on the GPM DPR was used for comparison [36]. The SLH-based APLH over the slope in spring also shows a clear dependence on terrain, whereas in summer it remains largely terrain-independent (Supplementary Fig. 14). This pattern is broadly consistent with our VPH-based results. However, SLH relies on rain type classification, and it carries relatively large uncertainties over the plateau's steep-slope region [24]. In contrast, the VPH approach—built on the strong linear relationship between the vertical gradient of rain rate and LH—cloud be better suited for the topographically complex plateau region.

To ensure the physical interpretability of the NO_SH experiment in spring, we conducted additional validation analyses. Removing slope SH induces near-surface (10 m) downslope flow near the Himalayan slopes (Supplementary Fig. 15b), a physically expected response to reduced surface heat fluxes and the associated 2-m cooling (Supplementary Fig. 15h). This subsidence weakens substantially by 900 hPa and becomes negligible by 800 hPa (Supplementary Fig. 15d,f), and the induced cooling also remains largely confined to the boundary layer with little impact at higher levels (Supplementary Fig. 16b). In spring NO_SH experiment, although ascent over the slope is weaker than in CON (Supplementary Fig. 11e), terrain-induced lifting still sustains an ascent-dominated circulation, with the strongest updrafts over higher-elevation terrain (>2 km). Consequently, LH over the higher-elevation slopes continues to closely follow the topography (Supplementary Fig. 6e).

Integrated satellite observations, reanalysis data, and WRF modeling diagnostics reveal the terrain-monsoon seesaw effect on governing seasonal precipitation regimes (Fig. 5).During the pre-monsoon spring period, terrain-dependent processes dominate: surface SH controls convective initiation below 2 km elevation, while orographic mechanical lift governs precipitation generation above 2 km. In contrast, the summer monsoon regime features large-scale SASM circulation overriding these local controls, driving depth-uniform convection that homogenizes the APLH independently of slope steepness.

The LH feature during summer cloud reassess moisture transport mechanisms to the TP .The observed summer APLH at 5–6 km demonstrates that plateau thermal forcing does not drive direct upslope transport of moisture-laden air from the Indian lowlands. These results validate Dong et al.'s [20] high-altitude inflow hypothesis while challenging slope-focused models [13, 14, 16]. Such terrain independence is difficult to reconcile with a "direct upslope" pathway in which near-surface, moisture-laden air is lifted from the foothills onto the plateau; if that mechanism prevailed, precipitation-related LH would be expected to show a much stronger topographic dependence. Instead, the results suggest monsoon-driven mid-tropospheric (~6 km) moisture advection (Supplementary Fig. 17), transporting southern moisture onto the plateau to trigger precipitation and the associated LH release. Crucially, the APLH-Coupling (Fig. 5b) demonstrates that Himalayan precipitation could constitutes the northernmost extension of the monsoonal convective system, not a locally forced phenomenon. The summer topographic decoupling of LH further indicates that the thermal pump is more closely tied to mid-tropospheric air masses (~6 km) over

the Indian subcontinent (and potentially farther upstream), and that it facilitates the advection of warm, moist southerly flow toward the plateau through a pumping-induced inflow. Our study provides the first observational evidence for the vertical level at which the thermal pump most effectively operates, offering a fresh observational perspective that may help refine the understanding of this complex issue in the monsoon debate.

This paradigm shift enables LH profiles within precipitation clouds to be used as dynamic tracers of convective processes. LH-based diagnosis of terrain–circulation interactions also offers guidance for identify how the impact of topography–monsoon seesaw shapes precipitation over global giant mountainous terrain, such as the Alps in the central Europe, the Andes in the western coast of South America, and the Rockies in North America, where their regional hydrological cycles and interactions are intense and significant for the human social economic production. While accurate prediction of summer rainfall over the TP remains a major challenge, recent studies have indicated that incorporation of physical constraints via observations is essential to reducing uncertainties in SASM and precipitation projections under different climate scenarios [37-39]. Consequently, by providing direct satellite-based constraints of the vertical LH structure, a new diagnostic benchmark is promising for the further improvement of terrain-monsoon interaction simulation, and monsoon rainfall prediction in climate models.

Methods

Core data. Global Precipitation Mission [40] Satellite orbit-level Vertical Profile Heating (VPH) data for the period 2014–2020 were used in this study [24]. This method is now also the operating algorithm for LH retrieval of the Chinese Fengyun-3G satellite (https://data.nsmc.org.cn/DataPortal/en/data/detail.html). For GPM products, LH profiles are retrieved by leveraging the strong correlation between the vertical gradient of rain rate (−dR/dZ) and LH, which has been validated over the TP. The dataset has a vertical resolution of 125 m and a horizontal resolution of approximately 5 km. Orbit-level LH and precipitation data were further aggregated to a $0.25° \times 0.25°$ grid by averaging all samples within each grid cell. Moisture and wind fields were obtained from the fifth-generation ECMWF reanalysis (ERA5) [41]. Topographic information was extracted from the 1-arc-minute global ETOPO dataset provided by the U.S. National Geophysical Data Center [42] and regridded to $0.25° \times 0.25°$ to match the LH data resolution. Additional dataset specifications are summarized in Supplementary Table 1.

Study domain. To assess the influence of Himalayan topography on the vertical structure of LH, four representative regions were selected following Fu et al. [43] and Zhang et al. [44]. The Flat Gangetic Plains (FGP) and the Foothills of the Himalayas (FHH) are characterized by elevations below 0.5 km, whereas the Himalayan–Tibetan Plateau Tableland (HTPT) lies above 5 km. The Steep Southern Slope of the Himalayas (SSSH), located between HTPT and FHH, exhibits the strongest topographic gradient, rising from ~0.5 km to over 4 km. Each region is delineated using

boundary curves aligned approximately parallel to the Himalayan ridge, facilitating comparisons of orographic effects on LH. Given the rapid elevation change across SSSH, it is further divided into three sub-regions: a low-elevation zone (<2 km; SSSH_low), a mid-elevation zone (2–4 km; SSSH_middle), and a high-elevation zone (>4 km; SSSH_high). Furthermore, to compare the vertical structures of precipitation and LH in different regions, a vertical cross section is selected, as indicated by A-A' line spanning four regions in Fig. 1a.

WRF simulations. Weather Research and Forecasting (WRF) simulations were performed for 2015 using a one-way nesting approach, with a high-resolution inner domain (10 km) embedded within a coarser outer domain (30 km; Supplementary Fig. 4). Because 2015 represents the weakest SASM year within our study period (2014–2020), as reported by the India Meteorological Department, it provides a stringent test case for assessing monsoon influences on precipitation processes over the southwestern Himalayas. Detailed model configurations and physical parameterization schemes are summarized in Supplementary Table 3. In the sensitivity experiments, the NO_HIM experiment removes the southern slope below 5.5 km, while the NO_SH experiment sets the surface sensible heat flux to zero over the same region by modifying the land surface scheme in WRF. The 20%SASM experiment is designed by reducing the lateral boundary wind speed and moisture over the core South Asian summer monsoon region by 80% and 40%, respectively.

Acknowledgements

This work was supported by the National Key Research and Development Program of China (Grant No. 2024YFF0809401), the National Natural Science Foundation of China NSFC (Grant No. 42330602, 42275139, 41830104), Innovation Center for Fengyun Meteorological Satellite Special Project (Grant no. FY-APP-ZX-2022.0211).

The authors acknowledge using DeepSeek-R1 (https://www.deepseek.com) for language polishing to enhance grammatical accuracy. All scientific content and interpretations remain solely the responsibility of the authors.

Data availability

The ERA5 reanalysis data used in this study are publicly available from the Copernicus Climate Data Store (https://cds.climate.copernicus.eu/datasets). Precipitation rate data derived from the GPM DPR are available from NASA Earthdata (https://search.earthdata.nasa.gov/). The VPH dataset is available from the corresponding author upon reasonable request.

Competing interests

The authors declare no competing interests

Chun Zhao is an Associate Editor of *npj Climate and Atmospheric Science* and was not involved in the journal's review of, or decisions related to, this manuscript.

References

1. Yao, T., Thompson, L. & Yang, W. *et al*. Different glacier status with atmospheric circulations in Tibetan Plateau and surroundings. *Nat. Clim. Chang.* **2**, 663–667 (2012).
2. Yao, T., Xue, Y. & Chen, D. *et al.* The imbalance of the Asian water tower. *Nat. Rev. Earth Environ.* **3**, 618–632 (2022).
3. Chen, D., Xu, B., Yao, T. *et al*. Assessment of past, present and future environmental changes on the Tibetan Plateau. *Chin. Sci. Bull*. **60**, 3025–3035 (2015).
4. Cheng, T. F., Chen, D. & Wang, B. *et al.* Human-induced warming accelerates local evapotranspiration and precipitation recycling over the Tibetan Plateau. *Commun. Earth Environ.* **5**, 388 (2024).
5. Lee, H., Calvin, K., Dasgupta, D. *et al*. Climate Change 2023: Synthesis Report. Summary for Policymakers. Intergovernmental Panel on Climate Change (IPCC), Geneva, Switzerland (2023).
6. Chen, X., Yuan, L. & Ma, Y. *et al.* A doubled increasing trend of evapotranspiration on the Tibetan Plateau. *Sci. Bull*. **69**, 1980–1990 (2024).
7. Chen, Z., Zhou, T. & Chen, X. *et al*. Observationally constrained projection of Afro-Asian monsoon precipitation. *Nat. Commun*. **13**, 2552 (2022).
8. Yan, H., Huang, J. & He, Y. *et al*. Atmospheric water vapor budget and its long-term trend over the Tibetan Plateau. *J. Geophys. Res. Atmos.* **125**, e2020JD033297 (2020).
9. Chen, F., Man, W. & Wang, S. *et al.* Southeast Asian ecological dependency on Tibetan Plateau streamflow over the last millennium. *Nat. Geosci*. **16**, 1151–1158 (2023).
10. Xu, F., Zhang, G. & Woolway, R. I. *et al.* Widespread societal and ecological impacts from projected Tibetan Plateau lake expansion. *Nat. Geosci.* **17**, 516–523 (2024).
11. Acosta, R. P. & Huber, M. Competing topographic mechanisms for the summer Indo-Asian monsoon. *Geophys. Res. Lett.* **47**, e2019GL085112 (2020).
12. Sha, Y., Shi, Z. & Li, X. *et al*. Distinct orographic controls on the asymmetrical onset of the South Asian summer monsoon: Hindu Kush versus Himalaya–Tibet. *J. Clim*. **36**, 6649–6667 (2023).
13. Wu, G., Duan, A. & Liu, Y. *et al*. Tibetan Plateau climate dynamics: recent research progress and outlook. *Natl. Sci. Rev*. **2**, 100–116 (2015).
14. Wu, G., Liu, Y. & He, B. *et al*. Thermal controls on the Asian summer monsoon. *Sci. Rep*. **2**, 404 (2012).
15. Chen, X., Xu, X. & Ma, Y. *et al*. Investigation of precipitation process in the water vapor channel of the Yarlung Zangbo Grand Canyon. *Bull. Am. Meteorol. Soc*. **105**, E370–E386 (2024).
16. Boos, W. R. & Kuang, Z. Dominant control of the South Asian monsoon by orographic insulation versus plateau heating. *Nature* **463**, 218–222 (2010).
17. Qiu, J. Monsoon melee. *Nature* **493**, 131–132 (2013).
18. Liu, Y., Lu, M. & Yang, H. *et al*. Land–atmosphere–ocean coupling associated with the Tibetan Plateau and its climate impacts. *Natl. Sci. Rev*. **7**, 534–552 (2020).

19. Lu, M., Yang, S., Wang, J., Wu, Y., & Jia, X. Response of regional Asian summer monsoons to the effect of reduced surface albedo in different Tibetan Plateau domains in idealized model experiments. *J. Clim*. **34**, 7023–7036 (2021).
20. Dong, W., Lin, Y. & Wright, J. S. *et al*. Summer rainfall over the southwestern Tibetan Plateau controlled by deep convection over the Indian subcontinent. *Nat. Commun.* **7**, 10925 (2016).
21. Chen, J., Xu, J., Wu, Z., et al. Decreased dust particles amplify the cloud cooling effect by regulating cloud ice formation over the Tibetan Plateau. Sci. Adv. **10(**37**)**, eado0885 (2024).
22. Yu, W., Guo, R., Thompson, L. G., et al. Water isotope ratios reflect convection intensity rather than rain type proportions in the pantropics. Sci. Adv. **10**(33), eado3258. (2024).
23. Li, R., Min, Q. & Fu, Y. 1997/98 El Niño–induced changes in rainfall vertical structure in the east Pacific. *J. Clim.* **24**, 6373–6391 (2011).
24. Li, R., Shao, W. & Guo, J. *et al*. A simplified algorithm to estimate latent heat rate using vertical rainfall profiles over the Tibetan Plateau. *J. Geophys. Res. Atmos.* **124**, 942–963 (2019).
25. Zhao, H., Li, R. & Zhang, P. *et al*. Satellite-based fully connected neural network heating (FCNH) algorithm for estimating latent heating rate inside storms. *J. Geophys. Res. Atmos.* **128**, e2022JD038448 (2023).
26. Zhao, H., Yang, S. & Wu, Q. *et al*. Optimizing satellite-based latent heating rate profiling using a convolutional neural network heating (CNNH) algorithm. *IEEE Trans. Geosci. Remote Sens.* **62**, 1–15 (2024).
27. Yin, J. F., Wang, D. H. & Liang, Z. M. *et al*. Numerical study of the role of microphysical latent heat and surface heat fluxes in a severe precipitation event in the warm sector over southern China. *Asia-Pac. J. Atmos. Sci.* **54**, 77–90 (2018).
28. Pan, X., Nie, X., Li, H. *et al*. Assessing spatiotemporal characteristics of atmospheric water cycle processes over the Tibetan Plateau using the WRF model and finer box model. *Sci. Rep*. **14**, 4959 (2024).
29. Chen, Y., Sharma, S., Zhou, X., Yang, K., Li, X., Niu, X., Hu, X., & Khadka, N. (2021). Spatial performance of multiple reanalysis precipitation datasets on the southern slope of central Himalaya. Atmospheric Research, 250, 105365.
30. Qin, J., Li, W., Fan, Z., He, W., Sun, W., & Chen, S. (2021). Evaluation of the ERA5 reanalysis precipitation dataset ver mainland China. Journal of Hydrology, 592, 125960.
31. Thomas, T. M., Bala, G. & Srinivas, V. V. Characteristics of the monsoon low pressure systems in the Indian subcontinent and the associated extreme precipitation events. *Clim. Dyn*. **56**, 1859–1878 (2021).
32. Vishnu, S., Boos, W. R. & Collins, W. D. Historical and future trends in South Asian monsoon low pressure systems in a high-resolution model ensemble. *npj Clim. Atmos. Sci.* **6**, 182 (2023).
33. Karmakar, N., Boos, W. R. & Misra, V. Influence of intraseasonal variability on the development of monsoon depressions. *Geophys. Res. Lett.* **48**, e2020GL090425 (2021).
34. Norris, J., Carvalho, L. M. V., Jones, C., & Cannon, F. (2020). Warming and drying over the central Himalaya caused by an amplification of local mountain circulation, NPJ Clim. Atmos. Sci., 3, 1.

35. Fujinami, H., Fujita, K., Takahashi, N., Sato, T., Kanamori, H., Sunako, S., & Kayastha, R. B. (2021). Twice‐daily monsoon precipitation maxima in the Himalayas driven by land surface effects. Journal of Geophysical Research: Atmospheres, 126(13), e2020JD034255.
36. GPM SLH Algorithm Development Team. (2022). Spectral Latent Heating (SLH) for TRMM/GPM: Algorithm Theoretical Basis Document (ATBD), Algorithm Ver. 07A (May 2022).
37. Hu, S., & Zhou, T. Skillful prediction of summer rainfall in the Tibetan Plateau on multiyear time scales. Sci. Adv. **7(**24**)**, eabf9395 (2021).
38. Huang, X., Zhou, T., Dai, A., et al. South Asian summer monsoon projections constrained by the interdecadal Pacific oscillation. Sci. Adv. 6(11), eaay6546 (2020).
39. Gao, Y., Hao, Q., Wang, L., et al. Changes in monsoon precipitation in East Asia under a 2 °C warming. Sci. Adv. **10 (**20), eadm7694 (2024).
40. GPM Science Team. GPM DPR spectral latent heat profiles L2 1.5 hours 5 km V05. *Goddard Earth Sciences Data and Information Services Center (GES DISC)* (2017).
41. Hersbach, H., Bell, B. & Berrisford, P. *et al*. ERA5 monthly averaged data on single levels from 1940 to present. *Copernicus Climate Change Service (C3S) Climate Data Store* (2023).
42. Amante, C. & Eakins, B. W. ETOPO1 1 Arc-Minute Global Relief Model: Procedures, data sources and analysis. *NOAA Tech. Memo. NESDIS NGDC* **24**, 1–19 (2009).
43. Fu, Y., Pan, X. & Xian, T. *et al.* Precipitation characteristics over the steep slope of the Himalayas in rainy season observed by TRMM PR and VIRS. *Clim. Dyn*. **51**, 1971–1989 (2018).
44. Zhang, A., Fu, Y., Chen, Y., Liu, G. & Zhang, X. Impact of the surface wind flow on precipitation characteristics over the southern Himalayas: GPM observations. *Atmos. Res.* **202**, 10–22 (2018).